

# Journal of Materials Chemistry C

Accepted Manuscript



This is an *Accepted Manuscript*, which has been through the Royal Society of Chemistry peer review process and has been accepted for publication.

*Accepted Manuscripts* are published online shortly after acceptance, before technical editing, formatting and proof reading. Using this free service, authors can make their results available to the community, in citable form, before we publish the edited article. We will replace this *Accepted Manuscript* with the edited and formatted *Advance Article* as soon as it is available.

You can find more information about *Accepted Manuscripts* in the [Information for Authors](#).

Please note that technical editing may introduce minor changes to the text and/or graphics, which may alter content. The journal's standard [Terms & Conditions](#) and the [Ethical guidelines](#) still apply. In no event shall the Royal Society of Chemistry be held responsible for any errors or omissions in this *Accepted Manuscript* or any consequences arising from the use of any information it contains.

# Temperature Dependent Microwave Absorption of Ultrathin Graphene Composites

Wen-Qiang Cao<sup>a,b</sup>, Xi-Xi Wang<sup>a</sup>, Jie Yuan<sup>b\*</sup>, Wen-Zhong Wang<sup>b\*</sup> and Mao-Sheng Cao<sup>a,\*</sup>

<sup>a</sup>School of Material Science and Engineering, Beijing Institute of Technology, Beijing 100081, China

<sup>b</sup>School of Science, Minzu University of China, Beijing 100081, China

## Abstract

Ultrathin graphene composites, with light weight, possess high-efficiency microwave absorption at elevated temperature as well as thermal-stability permittivity. The minimum reflection loss reaches -42 dB and the widest bandwidth covers the whole X-band (-10 dB). More significantly, the composites possess one high-efficiency absorbing belt with the value  $\leq -15$  dB, as well as two 'islands' of the reflection loss  $\leq -17$  dB and -30 dB. These excellent properties arise from the synergistic effect of polarization and conductivity. Our finding demonstrates that ultrathin graphene is a promising microwave absorber in microwave attenuation devices, information security and electromagnetic pollution defense, etc.

## 1. Introduction

Microwave absorber with lightweight and high efficiency in thermal-hash environment has aroused intensive interest of researchers due to various applications in the fields of communication, microwave devices, information security and electronic countermeasures, electromagnetic pollution defense and healthcare, etc.<sup>1-3</sup>

Up to date, plenty of new-type materials have been developed extensively and their microwave absorption properties are renewing rapidly.<sup>4-8</sup> The conducting polymer<sup>9</sup> and nonmagnetic metal<sup>10</sup> have potential in microwave absorption, but their microwave absorption

\*Corresponding author.

properties are usually not stable at elevated temperature. Although magnetic metal nickel and its oxides, such as urchin-like Ni<sup>11</sup> and NiO octahedral<sup>12</sup>, possess good microwave absorption properties, their applications are always limited by low Curie temperature. Other magnetic metals and their alloys with relatively high Curie temperature have been investigated extensively, including Fe cubes,<sup>13</sup> Co<sub>x</sub>Fe<sub>1-x</sub> alloy,<sup>14</sup> etc. However, their magnetism and conductivity decrease with increasing temperature, leading to the decrease of their microwave absorption. As for oxides and heterostructures, such as dendrite-like Fe<sub>3</sub>O<sub>4</sub>,<sup>15</sup> and Fe<sub>3</sub>O<sub>4</sub>@TiO<sub>2</sub> core-shell microspheres,<sup>4</sup> the microwave absorption properties of these materials need to be further improved, due to the degradation of their magnetism at elevated temperature. Hence, searching for microwave absorbers with stable or even enhanced microwave absorption properties in harsh-thermal environment is still a great challenge.<sup>16, 17</sup>

Carbon nanomaterials as well as their heterostructures, including carbon nanosheets,<sup>18, 19</sup> carbon fibers,<sup>20,21</sup> carbon nanocoils,<sup>22-24</sup> and carbon nanotubes,<sup>25-27</sup> exhibit strong microwave attenuation. For example, Tang et al.<sup>22, 23</sup> and Qin et al.<sup>24</sup> developed carbon nanocoils (including plait-like and twin carbon nanocoils) and carbon nanocoils decorated with Fe<sub>3</sub>O<sub>4</sub> and Al<sub>2</sub>O<sub>3</sub>, finding that carbon nanocoils were potential in microwave absorption with the minimum reflection loss (*RL*) ranging from ~ - 20 dB to ~ - 35 dB; Peng et al.<sup>27</sup> and Che et al.<sup>1</sup> investigated the microwave absorption properties of carbon nanotubes and their heterostructures (Fe encapsulated within carbon nanotubes) and found the *RL* of these materials ranging from ~ - 25 dB to ~ - 45 dB. It has been reported that graphene is a novel carbon material for microwave attenuation with high loss tangent, due to its extremely high specific surface area and carrier mobility, abundant defects and hydroxyl, epoxy and carboxyl groups.<sup>28-30</sup> For example, Chen and Huang et al. reported that the graphene foam exhibited microwave absorption performance with the *RL* less than ~ -38 dB in 2-18 GHz.<sup>28</sup> However, the microwave absorption property of graphene materials in thermal-harsh environment has

not been reported.

Herein, we fabricated ultrathin graphene, investigated the permittivity and microwave absorption of the ultrathin graphene composites in temperature range from 323 K to 473 K and in X-band for the first time, and discussed the mechanism. The excellent microwave absorption confirmed that the as-prepared ultrathin graphene is a promising candidate for lightweight and high-efficiency microwave absorber in thermal-hash environment.

## 2. Experimental

### 2.1 Materials

Graphene oxide was obtained by harsh oxidation of the commercial graphite powder according to the modified Hummers' method.<sup>31, 32</sup> Subsequently, the ultrathin graphene was produced by solution-based reduction of graphene oxide with hydriodic acid and acetic acid, and then freeze-dried. Detail processes are shown in Fig.S1†.

### 2.2 Fabrication of Ultrathin Graphene/SiO<sub>2</sub> composites

The as-prepared graphene powders (3 wt.%, 7 wt.% and 11 wt.% in the composites) were individually mixed with silica-xerogel powders and then pressed into rectangular dimensions of 22.86 mm×10.16 mm×~1.7 mm with a cold press under 20 MPa pressure for dielectric measurements.

### 2.3 Characterization

The XRD patterns were collected on an X'Pert PRO system (Cu-K $\alpha$ ). The Raman spectra was obtained on a HORIBA JobinYvon HR800 Raman spectrometer equipped with a Spectra-Physics Ar-Kr laser source for 647 nm excitation and an Olympus BX-41 microscope. The X-ray diffraction and Raman patterns exhibit typical graphene structure, shown in Fig.S2†. The TEM images were obtained on a JEM-2100, coupled with carbon- or holey carbon-coated copper grids. The SEM patterns were taken on a HITACHI S-4800 microscope

and the AFM patterns were collected on a Veeco Dimension FastScan system, a typical supporting data shown in Fig. S3†.

#### 2.4 Electrical, dielectric property and microwave absorption

The DC conductivity measurements of the samples (with painted silver electrodes) were carried out using a Keithley 2401A-6517B multi-meter, as a set of supporting data shown in Fig. S4†.

The relative complex permittivity of samples, with the real part of the permittivity  $\epsilon'$  and the imaginary part  $\epsilon''$ , was determined by a vector network analyzer (VNA) (Anritsu37269D) using the wave-guide method at elevated temperatures between 323K and 473K in the X-band.<sup>17, 33</sup> The sample sheet positioned vertically in the center of test chamber was heated by an inner heater at 20 K/min while the distance between the sample and the microwave probe is 64mm. In the procedure, a period of 25 min was required for the system to stabilize when each set-point temperature was achieved in order to ensure the accuracy of measurement. Then the next set of duplicate measurements was followed. This process went on until the data covering the whole temperature range was obtained.

The reflection loss  $R_L$  of the sample is calculated according to transmission line theory to evaluate the microwave absorption. The  $R_L$  can be evaluated as

$$R_L = 20 \log \frac{|Z_{in} - 1|}{|Z_{in} + 1|} \quad (1)$$

Here the normalized input impedance  $Z_{in}$  of microwave absorption layer can be expressed as

$$Z_{in} = \sqrt{\frac{\mu_r}{\epsilon_r}} \tanh \left[ j \frac{2\pi}{c} \sqrt{\mu_r \epsilon_r} f d \right] \quad (2)$$

where  $c$  is the light velocity in vacuum,  $f$  the microwave frequency,  $d$  the thickness of the absorber,  $\epsilon_r$  and  $\mu_r$  the relative permittivity and permeability of the sample, coming from the experimental data.

### 3. Results and discussion

Fig. 1A-C is the scanning electron microscope (SEM) images of the graphite, graphite oxide and graphene, respectively. The flake graphite used as the precursor, is shown in Fig. 1A. The graphite is multilayer and plain, which can be further confirmed by Fig. 1D. According to the modified Hummers' method, the graphite oxide was obtained by adding the deionized water to the reaction vessel. As shown in Fig. 1B, the graphite oxide is also multilayer but more flexible than graphite, and some parts are bended. Fig. 1E is the SEM image of 3-4 graphite oxides stacking together, and Fig. 1G-I is the enlarged images of the graphite oxide, indicating the graphite layers are separating. When the graphite is harsh oxidized, the functional groups are adhered on/into the graphite. This would make the distance of the interlamination to be increased, allowing the water molecules spread easily into the interlayer. The as-prepared graphene is shown in Fig. 1C and 1F. The graphene is much thinner with wrinkle.

Fig. 2A and 2B are the transmission electron microscope (TEM) images of the graphite and graphene, and demonstrate the thickness of the layers decreased through the fabrication, which can be confirmed by the following high-resolution electron microscope (HRTEM) and selected area electron diffraction (SAED) images. As observed from Fig. 2C, the graphite shows a typical graphite lattice fringe, and the distinct diffraction spots of graphite is also shown on the SAED pattern in Fig. 2E. The diffraction profile generated by the SAED pattern in Fig. 2E has four distinct graphite diffraction peaks, corresponding to the (002), (100), (004) and (110) crystal plane of the graphite. As for the graphene, Fig. 2D shows no lattice fringe, and Fig. 1F demonstrate the SAED pattern along the [001] zone axis depicts a weaker graphitic-crystal structure, indicating the layers decreased. In the diffraction profile of the graphene, a rather weak peak is observed at  $2\theta=42.76^\circ$ , corresponding to the (100) crystal plane of the graphene. It also demonstrates the extreme thinness of the graphene, which can

be further confirmed by atomic force microscope (Fig. S3†).

Fig. 3 shows the three dimensional (3D) plots of the reflection loss ( $RL$ ) of the composites versus frequency, temperature, selected thickness (1.5, 1.8, 2.1, 2.4 and 2.7 mm),  $\epsilon'$  and  $\epsilon''$ . Fig. 3A shows the 7 wt.% composite possesses a high absorbing belt with the  $RL \leq -15$  dB at 413K, and there are two excellent microwave absorption 'islands'. The  $RL$  of the two 'islands' are less than -17 dB and -30 dB, respectively. More significantly, their  $RL$  values are -23 dB and -42 dB. Fig. 3B demonstrates the  $RL$  of the 7 wt.% composite with a thickness of 2.4 mm versus frequency and temperature. There is an absorbing belt with the  $RL \leq -10$  dB, which almost covers the whole X-band and the temperature ranging from 323K to 473K. Meanwhile, Fig.3C shows the 3D projection plots of  $RL$  versus  $\epsilon'$  and  $\epsilon''$  with a thickness of 2.1 mm at 12.4 GHz. The red dots show the  $RL$  peaks of the 7 wt.% composite in measured temperature. The microwave absorption peaks of the graphene composites are much closer to the theoretical extreme point, which reveals that the microwave absorption is controllable by adjusting the  $\epsilon'$  and  $\epsilon''$  properly and tuned by frequency and temperature.

Fig.4 shows the microwave absorption curves of the ultrathin graphene composites. In Fig. 4A, the 7 wt.% composite has the lowest  $RL$  of -42 dB with a thickness of 2.1 mm at 413 K, compared with the 3 wt.% and 11 wt% composites. The 7 wt.% composite has the best microwave absorption properties versus temperature in Fig. 4B. The  $RL$  with the minimum values  $< -20$  dB covers the whole measured temperature at 12.4 GHz with a thickness of 2.1 mm. Fig. 4C exhibits the  $RL$  of the composite loaded with 7 wt.% graphene versus thickness at 413K. The bandwidth ( $RL \leq -10$ dB) covers almost the whole X-band with a thickness of 2.4 mm, which is better than those of the 3 wt.% and 11 wt% composites. The  $RL$  of the composite loaded with 7 wt.% graphene with a thickness of 2.4 mm at different temperatures was observed in Fig.4D. The result demonstrates that the widest bandwidth ( $RL \leq -10$  dB) of the composites covers almost the whole X-band.

The microwave absorption mechanism is illustrated in Fig. 5. Firstly, as shown in Fig. 5A, the dipoles are formed in electric field due to the functional groups and clustered defects introduced *via* the chemical conversion process. Meanwhile, the dipoles are not evenly distributed, and indexed to the orientation polarization and the relaxation loss. However, when temperature rises, the graphene composites turn into relaxed state. The decreasing internal friction causes the loss tangent. Secondly, in Fig. 5B, the capacitor-like junctions are formed owing to the increasing mass ratio, contributing to the polarization in electromagnetic field. These junctions can further increase the relaxation. Thirdly, the electron hopping increases with increasing temperature. The conductive network is formed in the ultrathin graphene composites when the mass ratio is over threshold. The electric loss increases with increasing temperature, as exhibited in Fig. 5C. Moreover, the scattered microwave by the corrugated graphene sheets has significantly enhanced attenuation of multiple internal reflection modes of the graphene composites in Fig. 5D. Meanwhile, the tunable microwave absorption is attributed to the impedance matching that controlled by the different graphene mass ratios as well as matching thickness of the graphene composites in changing temperature.<sup>34</sup> These variables lead to the change in the complex permittivity.

The mechanism of microwave absorption of the ultrathin graphene composites can be supported by the measured imaginary permittivity and loss tangent in Fig. 6. The imaginary permittivity exhibits similar temperature-dependent trend in Fig. 6A, 6C and 6E. For the 3 wt.% graphene composite, the imaginary permittivity decreases with increasing temperature. The relaxation presents main effect on the imaginary permittivity since the conductive network has not formed in composite, making the microwave absorption of the 3 wt.% graphene composite lower than those of other mass ratios. For 7 wt.% graphene composite, the conductive network is formed in composite, and the conductivity enhances with increasing temperature, which causes both of the relaxation and conductivity have effect on

the imaginary permittivity. Hence, as for the 7 wt.% graphene composite, the imaginary permittivity remains stable due to the balance between the increasing conductivity and decreasing relaxation with increasing temperature. As the mass ratio of graphene composite rising from 7 wt.% to 11 wt%, the conductivity of the composite continually enhances, causing the imaginary permittivity increases with increasing temperature, which can confirm that conductivity has obvious contribution to the imaginary permittivity. From Fig. 6B, 6D and 6F, it can be found that the characteristic of the loss tangent is similar to the imaginary permittivity. It means both the conductivity and relaxation have synergistic effect on the imaginary permittivity and loss tangent, as well as microwave absorption property.

According to Debye theory, the imaginary part  $\varepsilon''$  could be regarded as the complex contributions of both relaxation and conductance, described as the following:<sup>17, 33</sup>

$$\varepsilon''(\omega) = \varepsilon_p'' + \varepsilon_c'' = (\varepsilon_s - \varepsilon_\infty) \frac{\omega\tau}{1 + \omega^2\tau^2} + \frac{\sigma(T)}{\varepsilon_0\omega} \quad (3)$$

Where  $\sigma(T)$  is the temperature-dependence electrical conductivity,  $\omega$  the angular frequency,  $\tau$  the temperature-dependence relaxation time,  $\varepsilon_s$  the static permittivity and  $\varepsilon_\infty$  the relative permittivity.

Consequently,  $\varepsilon''$  contains two sections:  $\varepsilon_p''$  induced by relaxation and  $\varepsilon_c''$  induced by conductance. The ratios of the  $\varepsilon_c''$  to the  $\varepsilon''$  are illustrated in Fig. S4†, which presents strong temperature-dependence at elevated temperature.<sup>32, 35</sup> From Fig. S4†A, the low  $\varepsilon_c''$  has few effect on the  $\varepsilon''$  although it increases with increasing temperature. The  $\varepsilon_c''$  of the composites also increased as shown in Fig. S4†B and S4†C. It can be found that the  $\varepsilon_c''$  of the composites loaded with 7 wt.% and 11 wt% contributes to the  $\varepsilon''$  gradually with increasing mass ratio, which can be investigated in the three insets in Fig. S4†.

### 3. Conclusions

In summary, chemically graphitized ultrathin graphene exhibits high-efficiency microwave

absorption at elevated temperature. The maximum loss tangent and minimum reflection loss in X-band ranging from 323 to 473K, are 1.32 and -42 dB, respectively, and the widest bandwidth for  $RL \leq -10$  dB almost covers the whole X-band. The cooperation of dipole polarization and hopping conductivity is responsible for excellent microwave absorption of ultrathin graphene composites. Furthermore, the ultrathin graphene composites show typical temperature-dependence permittivity and microwave absorption. The composites with high carrier mobility may achieve versatile functionality, where polarization and conductivity are intrinsically linked. The excellent microwave absorption performance demonstrates that the ultrathin graphene provide potential application for many fields in thermal-harsh environment.

**Conflict of Interest:**

The authors declare no competing financial interest.

**Acknowledgment:**

This project was financially supported by the National Natural Science Foundation of P. R. China (Grant Nos. 51372282, 51072024 and 51132002).

**Reference**

- [1] R. C. Che, L. M. Peng, X. F. Duan, Q. Chen and X. L. Liang, *Adv. Mater.*, 2004, **16**, 401.
- [2] M. S. Cao, X. X. Wang, W. Q. Cao and J. Yuan, *J. Mater. Chem. C*, 2015, **3**, 6589.
- [3] C. Y. Liang, C. Y. Liu, H. Wang, L. N. Wu, Z. H. Jiang, Y. J. Xu, B. Z. Shen and Z. J. Wang, *J. Mater. Chem. A*, 2014, **2**, 16397.
- [4] J. W. Liu, R. C. Che, H. J. Chen, F. Zhang, F. Xia, Q. S. Wu and M. Wang, *Small*, 2012, **8**, 1214.
- [5] S. Biswas, G. P. Kar and S. Bose, *J. Mater. Chem. A*, 2015, **3**, 12413.
- [6] C. Y. Liu, Y. J. Xu, L. N. Wu, Z. H. Jiang, B. Z. Shen and Z. J. Wang, *J. Mater. Chem. A*,

- 2015, **3**, 10566.
- [7] G. Z. Wang, X. G. Peng, L. Yu, G. P. Wan, S. W. Lin and Y. Qin, *J. Mater. Chem. A*, 2015, **3**, 2734.
- [8] X. W. Yin, L. Kong, L. T. Zhang, L. F. Cheng, N. Travitzky and P. Greil, *Int. Mater. Rev.*, 2014, **59**, 326.
- [9] X. F. Lu, W. J. Zhang, C. Wang, T. C. Wen and Y. Wei, *Prog. Polym. Sci.*, 2011, **36**, 671.
- [10] J. Y. Dong, R. Ullal, J. Han, S. H. Wei, X. Ouyang, J. Z. Dong and W. Gao, *J. Mater. Chem. A*, 2015, **3**, 5285.
- [11] C. Wang, X. J. Han, P. Xu, J. Y. Wang, Y. C. Du, X. H. Wang, W. Qin and T. Zhang, *J. Phys. Chem. C*, 2010, **114**, 3196.
- [12] G. X. Tong, Q. Hu, W. H. Wu, W. Li, H. S. Qian and Y. Liang, *J. Mater. Chem.*, 2012, **22**, 17494.
- [13] X. Fan, J. G. Guan, Z. Z. Li, F. Z. Mou, G. X. Tong and W. Wang, *J. Mater. Chem.*, 2010, **20**, 1676.
- [14] Z. X. Yu, N. Zhang, Z. P. Yao, X. J. Han and Z. H. Jiang, *J. Mater. Chem. A*, 2013, **1**, 12462.
- [15] G. B. Sun, B. X. Dong, M. H. Cao, B. Q. Wei and C. W. Hu, *Chem. Mater.*, 2011, **23**, 1587.
- [16] H. J. Yang, M. S. Cao, Y. Li, H. L. Shi, Z. L. Hou, X. Y. Fang, H. B. Jin, W. Z. Wang and J. Yuan, *Adv. Opt. Mater.*, 2014, **2**, 214.
- [17] B. Wen, M. S. Cao, Z. L. Hou, W. L. Song, L. Zhang, M. M. Lu, H. B. Jin, X. Y. Fang, W. Z. Wang and J. Yuan, *Carbon*, 2013, **65**, 124.
- [18] F. S. Wen, H. Hou, J. Y. Xiang, X. Y. Zhang, Z. B. Su, S. J. Yuan and Z. Y. Liu, *Carbon*, 2015, **89**, 372.
- [19] Y. C. Qing, D. D. Min, Y. Y. Zhou, F. Luo and W. C. Zhou, *Carbon*, 2015, **86**, 98.
- [20] J. Xiang, J. L. Li, X. H. Zhang, Q. Ye, J. H. Xu and X. Q. Shen, *J. Mater. Chem. A*, 2014, **2**, 16905.
- [21] Z. Y. Chu, H. F. Cheng, W. Xie and L. K. Sun, *Ceram Int*, 2012, **38**, 4867.
- [22] N. J. Tang, Y. Yang, K. J. Lin, W. Zhong, C. T. Au and Y. W. Du, *J. Phys. Chem. C*, 2008, **112**, 10061.
- [23] N. J. Tang, W. Zhong, C. T. Au, Y. Yang, M. G. Han, K. J. Lin and Y. W. Du, *J. Phys. Chem. C*, 2008, **112**, 19316.
- [24] G. Z. Wang, Z. Gao, S. W. Tang, C. Q. Chen, F. F. Duan, S. C. Zhao, S. W. Lin, Y. H.

- Feng, L. Zhou and Y. Qin, *ACS Nano*, 2012, **6**, 11009.
- [25] Z. J. Wang, L. N. Wu, J. G. Zhou, Z. H. Jiang and B. Z. Shen, *Nanoscale*, 2014, **6**, 12298.
- [26] Y. H. Chen, Z. H. Huang, M. M. Lu, W. Q. Cao, J. Yuan, D. Q. Zhang and M. S. Cao, *J. Mater. Chem. A*, 2015, **3**, 12621.
- [27] H. Sun, R. C. Che, X. You, Y. S. Jiang, Z. B. Yang, J. Deng, L. B. Qiu and H. S. Peng, *Adv. Mater.*, 2014, **26**, 8120.
- [28] Y. Zhang, Y. Huang, T. F. Zhang, H. C. Chang, P. S. Xiao, H. H. Chen, Z. Y. Huang and Y. S. Chen, *Adv. Mater.*, 2015, **27**, 2049.
- [29] Z. P. Chen, C. Xu, C. Q. Ma, W. C. Ren and H. M. Cheng, *Adv. Mater.*, 2013, **25**, 1296.
- [30] J. J. Liang, Y. Wang, Y. Huang, Y. F. Ma, Z. F. Liu, J. M. Cai, C. D. Zhang, H. J. Gao and Y. S. Chen, *Carbon*, 2009, **47**, 922.
- [31] S. F. Pei, J. P. Zhao, J. H. Du, W. C. Ren and H. M. Cheng, *Carbon*, 2010, **48**, 4466.
- [32] B. Wen, M. S. Cao, M. M. Lu, W. Q. Cao, H. L. Shi, J. Liu, X. X. Wang, H. B. Jin, X. Y. Fang, W. Z. Wang and J. Yuan, *Adv. Mater.*, 2014, **26**, 3484.
- [33] M. S. Cao, W. L. Song, Z. L. Hou, B. Wen, J. Yuan, *CARBON*, 2010, **48**, 788
- [34] M. S. Cao, R. R. Qin, C. J. Qiu and J. Zhu, *Mater. Design*, 2003, **24**, 391.
- [35] J. Liu, W. Q. Cao, H. B. Jin, J. Yuan, D. Q. Zhang, M. S. Cao, *J. Mater. Chem. C*, 2015, **3**, 4670

### Figure captions

Fig. 1 SEM images of the (A, D) graphite, (B, E) graphite oxide, (G, H, I) magnified graphite oxide and (C, F) ultrathin graphene.

Fig. 2 TEM images of the (A) graphite and (B) ultrathin graphene, HRTEM images of the (C) graphite and (D) ultrathin graphene. SAED patterns of the (E) graphite and (F) ultrathin graphene.

Fig. 3 3D plots of microwave absorption properties of the ultrathin graphene composites, (A) the RL of the 7 wt.% composite at 413K versus thickness and frequency, (B) the RL of the 7 wt.% composite with a thickness of 2.4 mm versus temperature and frequency, (C) the RL of the idealized model with a thickness of 2.4 mm at 12.4 GHz versus real and imaginary permittivity.

Fig. 4 Microwave absorption properties of the ultrathin graphene composites, (A) the *RL* of the 3 wt.%, 7 wt.% and 11 wt% composites at 413K with a thickness of 2.1 mm versus frequency, (B) the *RL* of the 3 wt.%, 7 wt.% and 11 wt.% composites at 12.4 GHz with a thickness of 2.1 mm versus temperature, (C) the *RL* of the 7 wt.% composite at 413K with thickness of 2.1 mm, 2.4 mm and 2.7 mm versus frequency, (D) the *RL* of the 7 wt.% composite at 323 K, 413 K and 473K with a thickness of 2.4 mm versus frequency.

Fig. 5 Schematic illustrations for microwave absorption properties of the ultrathin graphene composites. (A) Polarization and relaxation, (B) forming capacitor-like structures, (C) the electronic transport and network, (D) microwave propagation model and wave scattering.

Fig. 6 The imaginary permittivity of the (A) 3 wt.%, (B) 7 wt.% and (C) 11 wt.% composites versus temperature, the loss tangent of the (D) 3 wt.%, (E) 7 wt.% and (F) 11 wt.%

composites versus temperature.

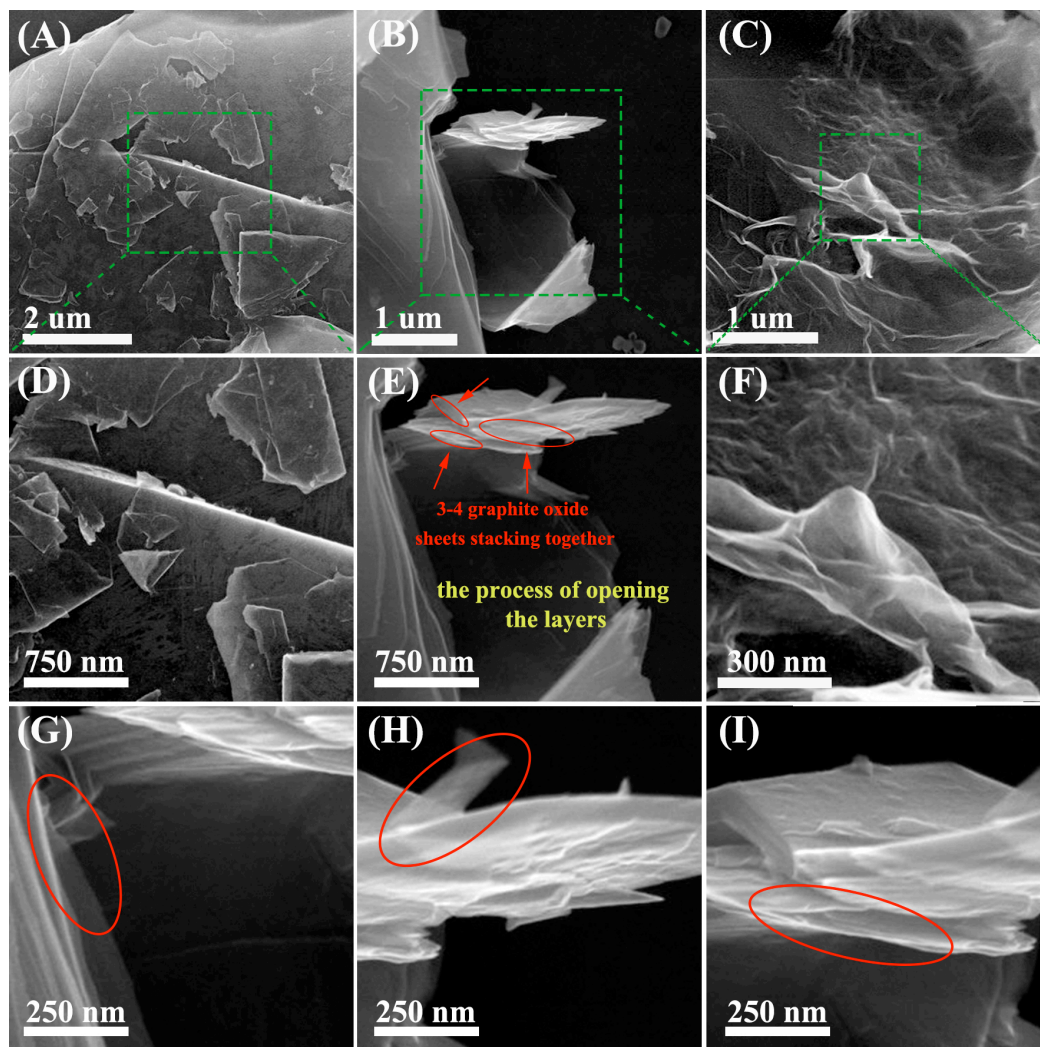


Fig.1

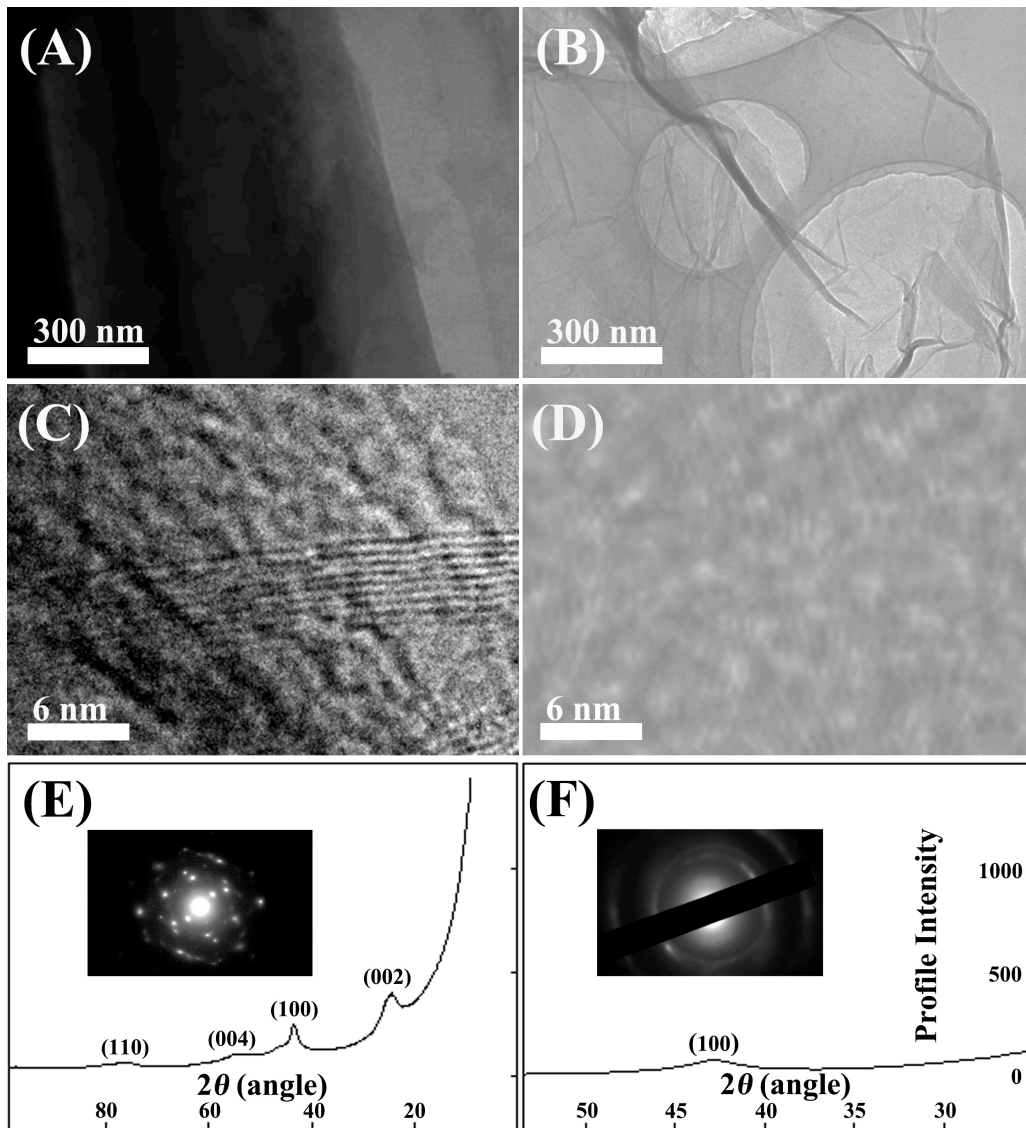


Fig.2

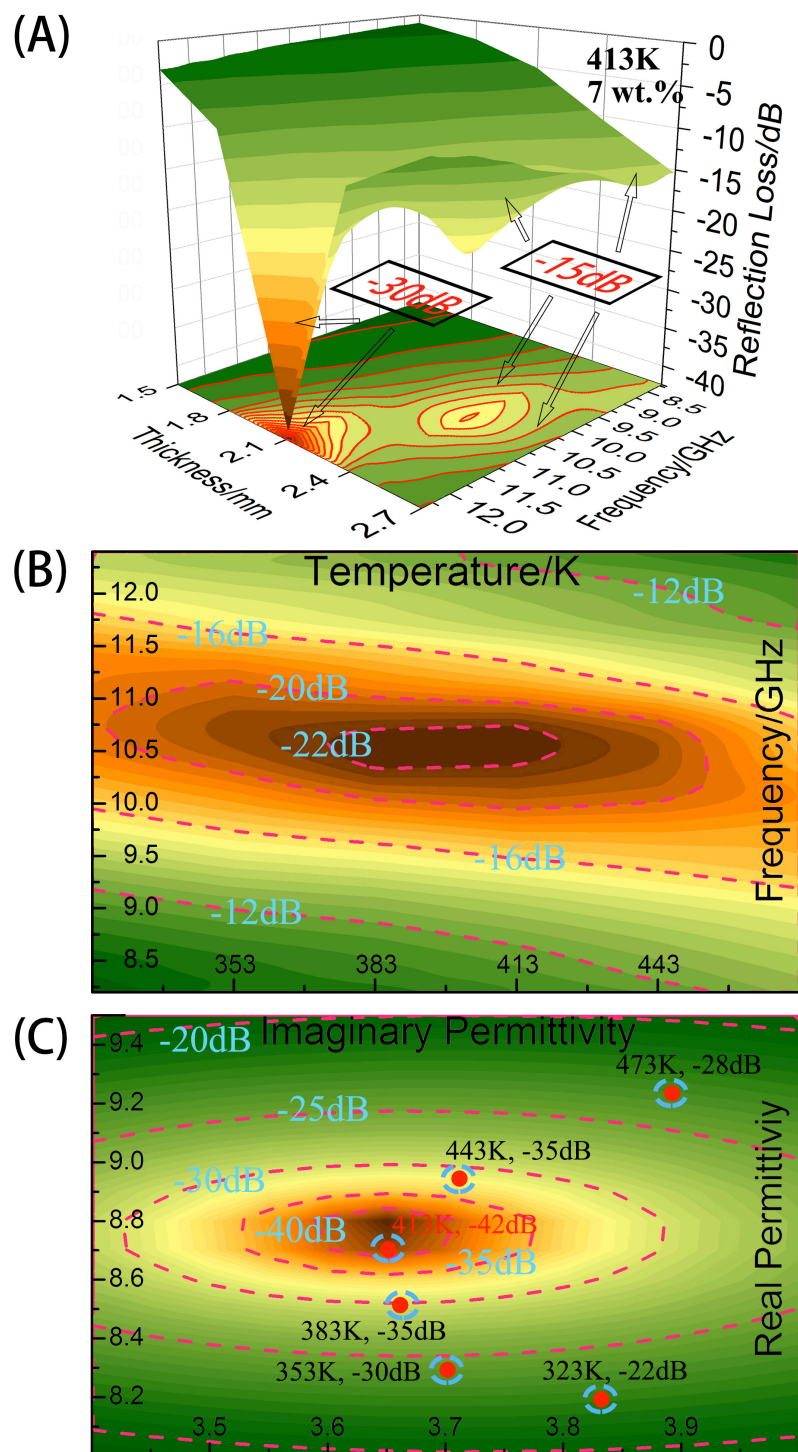


Fig.3

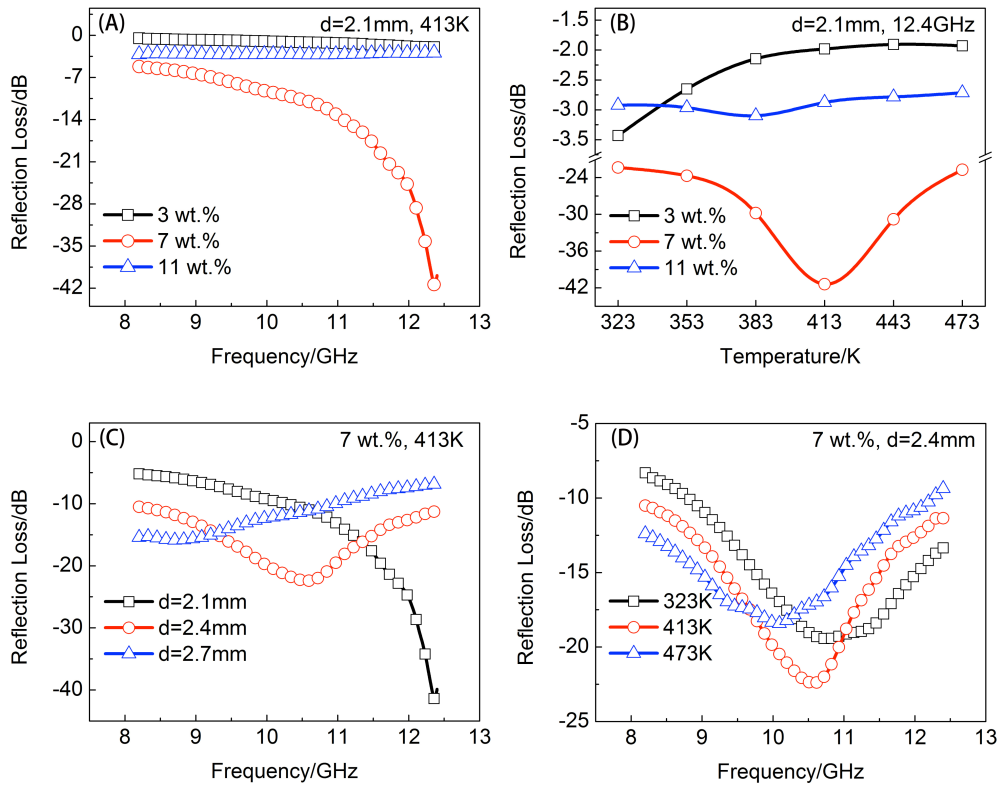


Fig.4

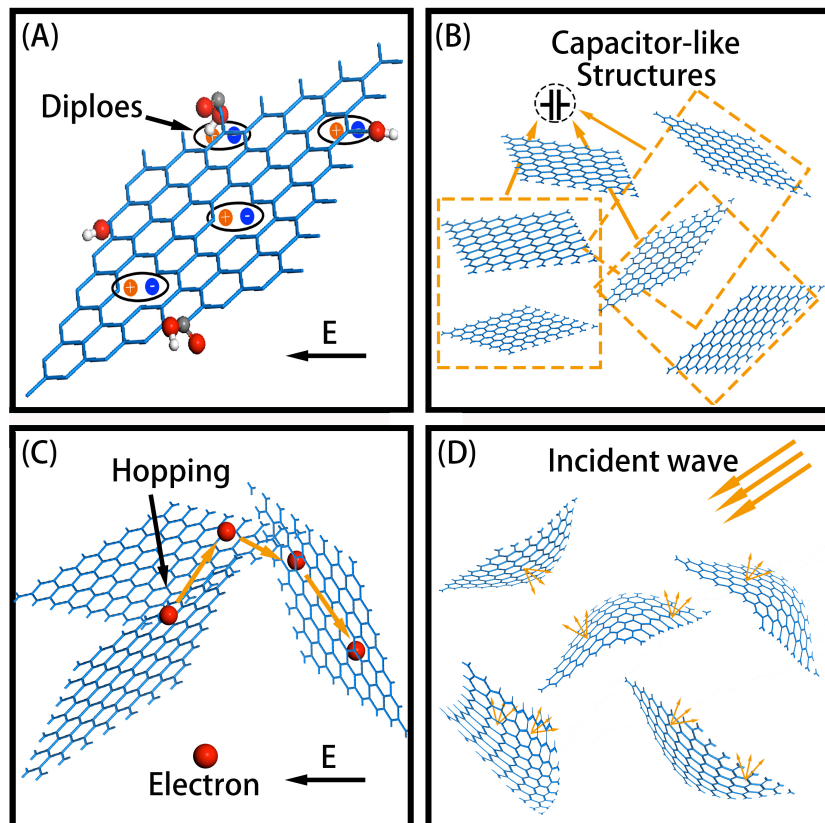


Fig.5

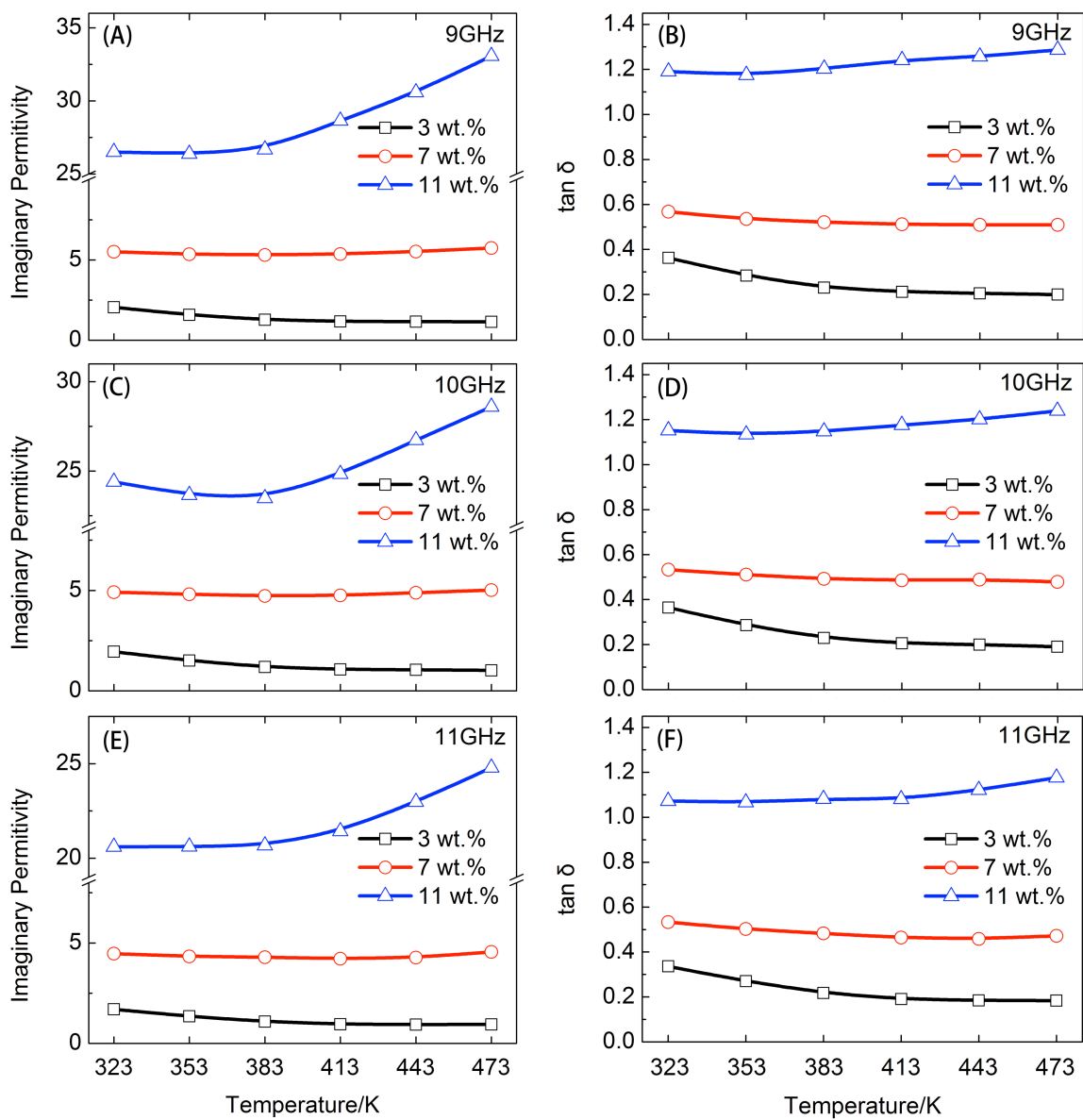
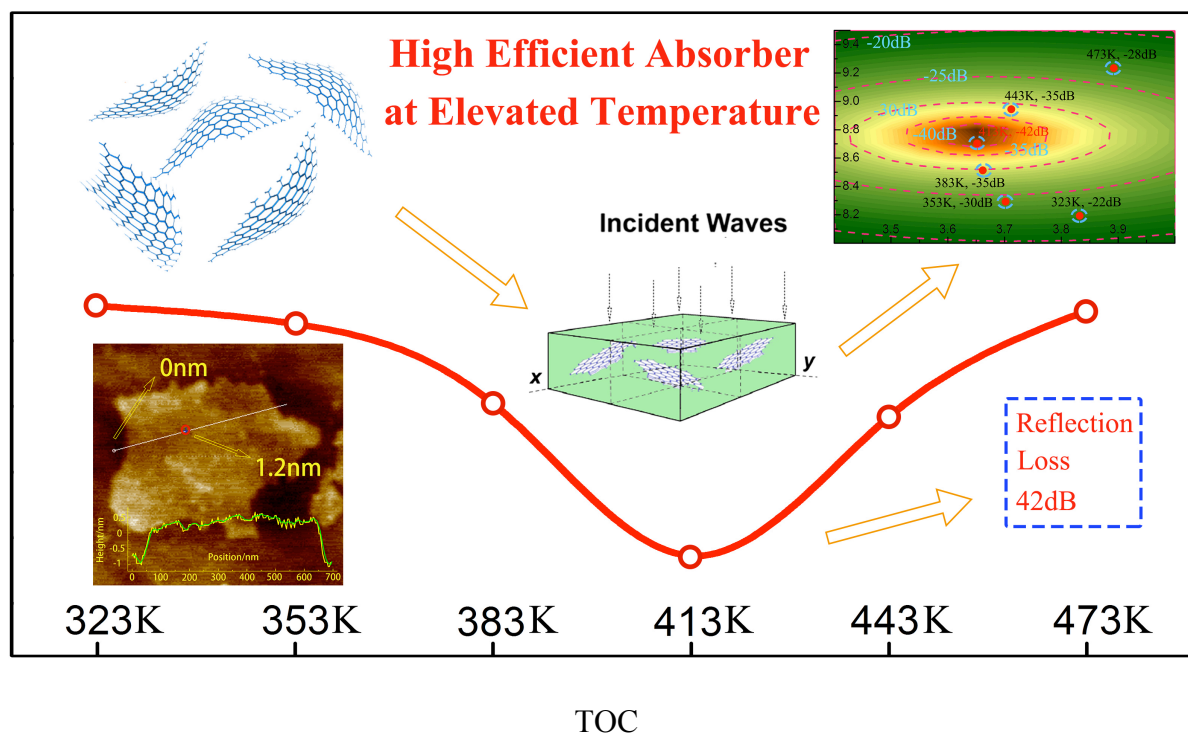
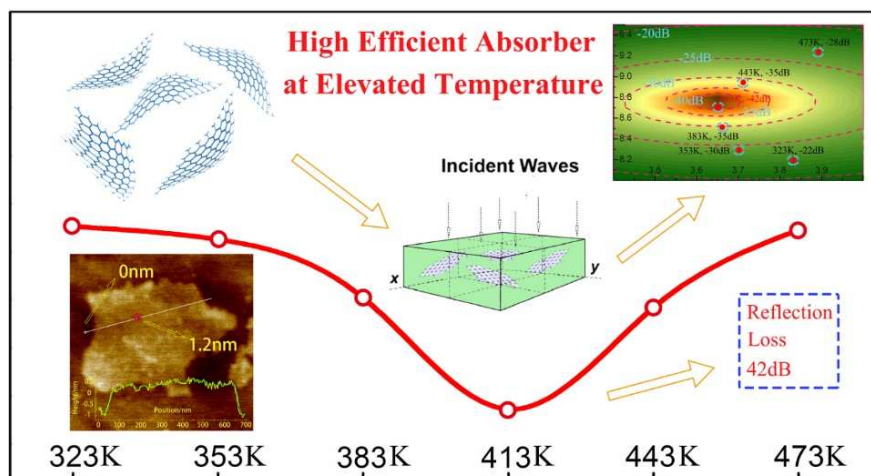


Fig.6



Chemical graphitized ultrathin graphene exhibits high-efficient microwave absorption at elevated temperature, attributed to the cooperation of dipole polarization and hopping conductivity. The ultrathin graphene composites show different dependences on changing concentrations and temperature towards imaginary permittivity and loss tangent value, as well as microwave absorptions.

## Graphical abstract



Chemical graphitized ultrathin graphene exhibits high-efficient microwave absorption at elevated temperature, attributed to the cooperation of dipole polarization and hopping conductivity. The ultrathin graphene composites show different dependences on changing concentrations and temperature towards imaginary permittivity and loss tangent value, as well as microwave absorptions.

\*Corresponding author.

Tel: +86 10 68914062. E-mail address: [caomaosheng@bit.edu.cn](mailto:caomaosheng@bit.edu.cn) (Mao-Sheng Cao); [wzhuangmuc@163.com](mailto:wzhuangmuc@163.com); [yuanjie4000@sina.com](mailto:yuanjie4000@sina.com)